

Attosecond-streaking time delays: Finite-range property and comparison of classical and quantum approaches

Jing Su,^{*} Hongcheng Ni, Andreas Becker, and Agnieszka Jaroń-Becker

JILA and Department of Physics, University of Colorado, Boulder, Colorado 80309-0440, USA

(Received 26 November 2013; published 13 January 2014)

We theoretically study time delays obtained using the attosecond-streaking technique. To this end, we compute time delays by numerically solving the corresponding time-dependent Schrödinger equation and analyze the delays using two classical methods, namely, a perturbative approach and a full numerical solution of Newton's equation describing the motion of the photoelectron in the continuum. A good agreement between the quantum streaking results and those from the full classical solution is found. This indicates that the streaking time delay arises from the continuum dynamics of the electron in the coupled potential of the Coulomb and streaking fields, while the transition of the photoelectron from the bound state to the continuum occurs instantaneously upon absorption of the photon. We further analyze the variation of the time delay with respect to the delay between the ionizing XUV pulse and a long streaking pulse, its dependence on the polarization direction of the streaking pulse, and the influence of the shape of the streaking pulse and/or additional static electric fields on the numerically obtained time delays. The results are interpreted based on the previously revealed property that the attosecond-streaking time delay depends on the finite region in space over which the electron propagates between its instant of transition into the continuum and the end of the streaking pulse.

DOI: [10.1103/PhysRevA.89.013404](https://doi.org/10.1103/PhysRevA.89.013404)

PACS number(s): 33.80.Rv, 33.80.Wz

I. INTRODUCTION

The development in laser technology in recent years, in particular, the generation of attosecond (as) extreme ultraviolet (XUV) laser pulses, has provided the possibility of observing and even controlling electron dynamics in atoms and molecules on an ultrafast time scale (for a recent review, see [1]). The attosecond streak camera technique [2] is an example of a method which is used to retrieve temporal information in ultrafast processes. The basic idea of this technique is that the momentum of a photoelectron, which is ionized by an ultrashort XUV pulse from a target, is streaked by an additional laser pulse, usually a near-infrared (IR) pulse. The final momentum of the electron then depends on the vector potential of the streaking field at the instant of the transition of the electron into the continuum. By scanning the relative delay between the two pulses, time information is mapped onto the streaking trace, i.e., the final electron momentum as a function of the relative delay between the two pulses.

In a recent application of the attosecond-streaking technique a temporal offset of 21 as between streaking traces of electrons emitted from $2s$ and $2p$ orbitals in a neon atom was reported by Schultze *et al.* [3]. This temporal offset was interpreted as the time delay between the emission of the $2s$ electron and that of the $2p$ electron. The observation initiated theoretical analysis of the origin of the measured temporal offset (e.g. [4–21]). Part of the debate is related to the role of the Wigner-Smith (WS) time delay [22,23], which is the time delay a particle accumulates in a potential compared to a free particle with the same asymptotic final momentum. However, for a long-range potential, such as the Coulomb interaction, the WS time delay diverges (e.g. [8–10,23]) and therefore cannot explain the observed finite streaking time delay. More recently, the temporal offset is often separated

into a sum of two contributions (e.g. [11–15]), namely, a WS time delay arising due to the short-range part of the potential, including multielectron effects (e.g. [4,15–17]) and potentially polarization effects (e.g. [8,18,19]), and a delay due to the coupling between the streaking field and the Coulomb field. For the latter contribution it has been discussed whether the short- and/or the long-range parts of the Coulomb potential have to be taken into account [11,14].

We have recently shown [21] that, alternatively, the observed time delay can be written as a sum or integral of piecewise field-free time delays weighted by the instantaneous streaking-field strength, relative to the streaking field strength at the instant of transition of the electron into the continuum. The analysis was based on results of quantum streaking simulations as well as of classical electron dynamics in the streaking field after the interaction with the XUV field. It led us to the interpretation that the observed time delay depends on the finite time between the transition into the continuum and the end of the streaking pulse (or, alternatively, the finite region in space along the polarization direction over which the electron propagates during this time interval). Among others, this insight removes concerns related to the divergence of the WS time delay from the theoretical analysis.

In the present article we study the following aspects related to the finite-range time delays. First, we compare the results of quantum streaking simulations obtained by solving the time-dependent Schrödinger equation (TDSE) with those of two classical approaches. These are the full numerical solution of the corresponding Newton's equation of the electron dynamics in the continuum as well as an approximate solution, in which perturbation theory is used to treat the Coulomb potential in first order. Our results support earlier conclusions [8,17,21] that full classical calculations can reproduce the quantum streaking results. On the other hand, the results of the perturbative approach deviate from both the full classical and the quantum results. This discrepancy is discussed in view of the interpretation of the temporal offsets and the role of

^{*}jing.su@colorado.edu

laser-potential coupling. In the second part of the paper we further address the relevance of the finite-range property of the streaking time delays and analyze, in particular, the role of the shape and the polarization direction of the streaking pulse as well as the influence of additional static electric fields on the temporal offsets.

The paper is organized as follows. In Sec. II we present the theoretical methods used to calculate the temporal offset (or time delay) in the streaking experiment, both quantum mechanically and classically. For the analysis based on classical physics, we have applied both a perturbative approach and the full numerical solution. The time delays obtained from these two classical formulas are then compared with the TDSE results. The good agreement between the results from the full numerical solution and those from the TDSE confirm previous conclusions that the streaking time delay arises from the electron dynamics in the coupled field of the streaking field and the atomic potential. The limitations of the perturbative approach are discussed as well. In Sec. III we show that for a long streaking pulse, time delays extracted from different cycles of the pulse can vary. We further illustrate, using two two-dimensional (2D) examples, the relevance of the polarization direction of the streaking field on the results. The influence of a pedestal in the streaking field as well as of an additional static field on the streaking time delay is also studied. We conclude with a summary of the results, in Sec. IV.

II. STREAKING SIMULATIONS AND CLASSICAL ANALYSIS

In this section we briefly review the techniques used to extract time offsets (or delays) from numerical simulations of a streaking experiment. We then continue to discuss two classical approaches to describing the dynamics of the photoelectron in the streaking field, in which either the effect of the Coulomb field of the parent ion is considered to first order using perturbation theory or its effect together with the coupling with the streaking field is fully taken into account.

A. Quantum streaking simulations

To simulate a streaking experiment, we used standard techniques to numerically solve the TDSE (Hartree atomic units, $e = m = \hbar = 1$, are used throughout the paper, unless otherwise stated),

$$i \frac{\partial \Psi(\mathbf{r}, t)}{\partial t} = \left[\frac{\mathbf{p}^2}{2} + V(\mathbf{r}) + [\mathbf{E}_{\text{XUV}}(t) + \mathbf{E}_s(t)] \cdot \mathbf{r} \right] \Psi(\mathbf{r}, t), \quad (1)$$

where \mathbf{p} is the momentum operator and

$$\mathbf{E}(t) = E_0 \sin^2(\pi t/T) \cos(\omega t + \phi) \hat{\mathbf{z}} \quad (2)$$

is the expression used for both the photoionizing XUV and the streaking laser fields, $\mathbf{E}_{\text{XUV}}(t)$ and $\mathbf{E}_s(t)$, respectively. Both fields are considered to be linearly polarized in the z direction, where E_0 is the peak amplitude, T is the pulse duration, ω is the central frequency, and ϕ is the carrier-envelope phase of the respective field. We solved the TDSE on a grid in space and time using the Crank-Nicolson method. In each simulation we propagated the wave function on the grid for a sufficiently long time until both laser pulses ceased and the ionized wave

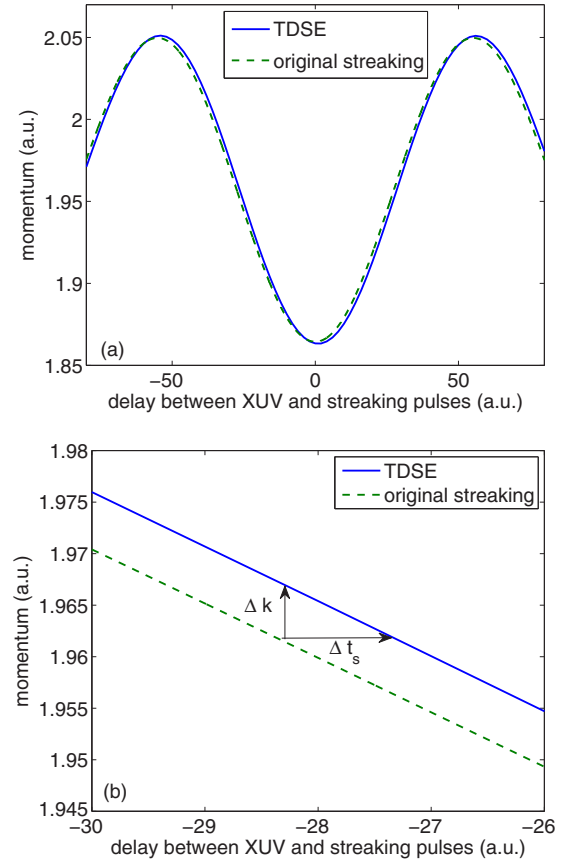


FIG. 1. (Color online) (a) Streaking traces obtained from numerical simulations for photoemission in the 1D Coulomb potential $V_C(z)$. An eight-cycle streaking pulse with $I_s = 1 \times 10^{12}$ W/cm², $\lambda_s = 800$ nm, and $\phi_s = -\pi/2$ was used in the calculations. We compare the streaking trace obtained from the TDSE [solid (blue) line] with that from the original streaking formula [Eq. (4); dashed (green) line]. (b) An enlargement of (a) to show the momentum shift Δk , the streaking time delay Δt_s , and the relation between them.

packet was far from the ionic core. We confirmed that in all simulations the outgoing wave packets stay on the grid and do not reach its boundaries.

To obtain the momentum distribution we spatially separated the ionized wave packet from the total wave function, which is possible due to the long propagation times used in the simulations, and then performed a Fourier transform. We have confirmed that the small error due to the projection onto the plane wave is negligible since we have propagated the ionized wave packet sufficiently far away from the nucleus. By varying the delay τ between the XUV and the streaking pulses, we obtained the streaking trace, in which the momentum of the photoelectron k_f is given as a function of τ .

An example for a streaking trace, over about the central cycle of an eight-cycle streaking pulse at 800 nm and 1×10^{12} W/cm², is shown in Fig. 1(a). In this set of simulations we used a 1D soft-core Coulomb-like potential, given by

$$V(z) = V_C(z) = -\frac{Z}{\sqrt{z^2 + a}} \quad (3)$$

centered at $z = 0$ with effective charge $Z = 3.0$ and soft-core parameter $a = 2.0$. Typical grid parameters used in the 1D

calculations were $\Delta z = 0.05$, $\Delta t = 0.01$, and $N = 280\,000$ (i.e., the grid extends from -7000 to 7000).

In Fig. 1(a) the numerical streaking trace (solid line) is compared with the predictions of the original streaking formula (dashed line) [2],

$$k_{f,z}^{(0)}(\tau) = k_{0,z} - A_s(\tau), \quad (4)$$

where $k_{0,z}$ is the streaking-field-free asymptotic momentum of the photoelectron and $A_s(\tau)$ is the vector potential of the streaking field at time τ . In the context of the present analysis it is often sufficient to study 1D systems, since we consider linearly polarized streaking pulses, and thus, the streaking field interacts with the electron along the polarization direction.

As has been pointed out before [e.g. [7,8,11,12,19]; see also the enlarged view in Fig. 1(b)], the numerically obtained distribution has a temporal offset Δt_s with respect to the vector potential at τ . This offset is related to a momentum shift Δk compared to the momentum given by the original streaking formula. In general, Δt_s can be approximately extracted by fitting the momentum components of the photoelectron as

$$k_f(\tau) = k_0 - \alpha A_s(\tau + \Delta t_s), \quad (5)$$

or as

$$k_{f,z}(\tau) = k_{0,z} - \alpha A_s(\tau + \Delta t_s), \quad (6)$$

in the case of a linearly polarized streaking pulse. α and Δt_s can be determined using the least-squares method. For further analysis it is useful to expand Eq. (6) to first order as

$$k_{f,z}(\tau) \simeq k_{0,z} - \alpha A_s(\tau) + \alpha E_s(\tau) \Delta t_s, \quad (7)$$

which is justified if $\omega_s \Delta t_s \ll 1$ since $A_s(\tau)$ has a sinusoidal shape. In this approximation the offset Δt_s can be then written as [for $E_s(\tau) \neq 0$]

$$\Delta t_s \simeq \frac{k_{f,z}(\tau) - k_{0,z} + \alpha A_s(\tau)}{\alpha E_s(\tau)}. \quad (8)$$

Results of classical calculations below suggest that τ coincides with the instant in time of the transition of the electron from the bound state to the continuum, t_i , which we also denote the time of ionization, and Δt_s depends on τ as well as the duration T_s of the streaking pulse.

B. Classical approaches

In the original streaking formula, Eq. (4), the effect of the interaction between the electron in the continuum and the parent ion is neglected. To analyze the role of the Coulomb potential as well as the coupling between the Coulomb potential and the streaking field on the observed momentum difference Δk and hence the temporal offset Δt_s , a classical analysis of the electron dynamics in the continuum turns out to be useful. For a linearly polarized streaking pulse the classical dynamics along the polarization direction is determined by

$$\frac{dk_z}{dt} = -E_s(t) - \frac{dV}{dz}. \quad (9)$$

1. Perturbative approach

One approach to solving Eq. (9) is to use perturbation theory by assuming $|E_s| \gg |\frac{dV}{dz}|$. To first order, the final asymptotic

momentum is then given by [assuming $A(t) = 0$ and $V(z) = 0$ for $t \rightarrow \infty$]

$$\begin{aligned} k_{f,z}^{(1)}(t_i) &= k_{f,z}^{(0)}(t_i) + \Delta k_{f,z}^{(1)}(t_i) \\ &= k_{i,z} - A_s(t_i) + \frac{V(z_i)}{k_{i,z}} + \int_{t_i}^{\infty} \frac{E_s(t)V(z^{(0)}(t))}{k_z^{(0)}(t)^2} dt \\ &\simeq k_{0,z} - A_s(t_i) + \int_{t_i}^{\infty} \frac{E_s(t)V(z^{(0)}(t))}{k_z^{(0)}(t)^2} dt, \end{aligned} \quad (10)$$

where $k_{0,z} = \sqrt{k_{i,z}^2 + 2V(z_i)} \simeq k_{i,z} + V(z_i)/k_{i,z}$ is, again, the streaking-field-free asymptotic momentum,

$$z^{(0)}(t) = z_i + [k_i - A_s(t_i)](t - t_i) + \int_{t_i}^t A_s(t') dt', \quad (11)$$

and

$$k_z^{(0)}(t) = k_{i,z} - A_s(t_i) + A_s(t) \quad (12)$$

are the zeroth-order solutions for the position and momentum of the electron. t_i , z_i , and $k_{i,z}$ are the initial time, position, and momentum of the electron after its transition into the continuum.

Please note that for a finite duration T_s of the streaking pulse, i.e., $E_s(t) = 0$ for $t \geq T_s$, the limits of the integral in Eq. (10) are finite. Assuming an instantaneous response of the electron to the ionizing XUV field in the streaking experiment, we set $\tau = t_i$. Upon this assumption, Eq. (8) yields

$$\Delta t_s \simeq \frac{(\alpha - 1)A_s(t_i) + \int_{t_i}^{T_s} \frac{E_s(t)V(z^{(0)}(t))}{[k^{(0)}(t)]^2} dt}{\alpha E_s(t_i)}. \quad (13)$$

We note that Eq. (10) is equivalent to Eq. (25) in Ref. [24], in which the authors used a quantum approach to calculate the momentum shift induced by the so-called Coulomb-laser coupling effect in laser-assisted photoionization based on the eikonal approximation. This result was latter adopted in Ref. [11] to study the influence of the streaking field on the measured time delay in a streaking experiment. However, one may note that, similarly to what we have done here, the formula derived in Ref. [24] was based on the assumption that the laser field is rather strong (e.g., 1.5×10^{14} W/cm² in one of the numerical examples in Ref. [24]), which is usually not applicable for a streaking experiment (streaking intensities are typically in the range of 1×10^{10} to 1×10^{12} W/cm²). Below we therefore compare the results of the perturbative approach with the numerical solution for classical electron dynamics in order to test the applicability of the perturbative approach.

2. Numerical solution

The use of perturbation theory can be avoided by integrating Eq. (9), which yields the final asymptotic momentum,

$$\begin{aligned} k_{f,z}(t_i) &= \sqrt{k_{i,z}^2 + 2V(z_i) - 2 \int_{t_i}^{\infty} E_s(t)k_z(t) dt} \\ &= \sqrt{k_0^2 - 2 \int_{t_i}^{\infty} E_s(t)k_z(t) dt}. \end{aligned} \quad (14)$$

Assuming an instantaneous response (i.e., $\tau = t_i$) and finite streaking pulse duration T , the temporal offset, Eq. (8), is then given by

$$\Delta t_s \simeq \frac{\sqrt{k_0^2 - 2 \int_{t_i}^T E_s(t) k_z(t) dt - k_0 + \alpha A_s(t_i)}}{\alpha E_s(t_i)}, \quad (15)$$

which can be solved numerically.

It has previously been pointed out that the results of streaking simulations strongly depend on the location of ionization, z_i [8,11], and/or matching the correct asymptotic conditions [13]. Accurate results can be obtained, e.g., by sampling the initial conditions in classical Monte Carlo calculations (see, e.g. [8]). In test calculations we have found that the results of such calculations can often be well reproduced by using the most probable position of the electron of the respective initial quantum state. To make use of the classical analysis, either in the perturbative approach or by direct numerical integration, we further determine the fitting parameter α such that the temporal offset Δt_s remains approximately constant for application of the ionizing XUV pulse over one cycle of the streaking pulse (see Fig. 2 in Ref. [21]).

C. Comparison of results from different approaches

In order to test the accuracy of the predictions of the two classical approaches we compare in Fig. 2 the results of quantum streaking simulations (black circles) for the temporal offset Δt_s with the classical predictions, Eq. (13) [dashed (blue) lines] and Eq. (15) [solid (red) lines], for photoionization of an electron in (a) the 1D Coulomb potential $V_C(z)$, Eq. (3), with $Z = 3.0$ and $a = 2.0$; (b) the combination of the 1D Coulomb and Gaussian potentials (the electron was initially bound in the ground state of the Coulomb potential),

$$V(z) = V_{CG}(z) = -\frac{Z}{\sqrt{z^2 + a}} + V_0 e^{-\left(\frac{|z-z_0|}{\sigma}\right)^2}, \quad (16)$$

with $Z = 3.0$ and $a = 2.0$ for the Coulomb potential and $V_0 = -0.5$ and $\sigma = 2.0$ for the Gaussian potential centered at z_0 ; and (c) a 3D Coulomb potential of the form

$$V(\mathbf{r}) = -\frac{Z}{r}, \quad (17)$$

with $Z = 1.0$ and 2.0 for the H atom and He ion, respectively.

The streaking time delays Δt_s in the 1D quantum simulations were obtained by scanning the central cycle of the streaking field and then fitting the trace using Eq. (6). To ionize the electron initially bounded in the 1D Coulomb potential, we have used an XUV pulse with $I_{XUV} = 1 \times 10^{15}$ W/cm², $\omega_{XUV} = 100$ eV, $T_{XUV} = 600$ as, and $\phi_{XUV} = -\pi/2$. The parameters of the streaking pulse were $I_s = 1 \times 10^{12}$ W/cm², $\lambda_s = 800$ nm, $N_s = 3$ [Fig. 2(a)] or $N_s = 8$ [Fig. 2(b)], and $\phi_s = -\pi/2$. The 3D quantum results in Fig. 2(c) were extracted from Ref. [8]. In the classical calculations we assumed a transition to the continuum at the center of the XUV pulse (i.e., $t_i = \tau = T_{XUV}/2$).

The comparison reveals that the results of the quantum streaking simulations (black circles) and the full classical calculations [solid (red) lines] are in excellent agreement with

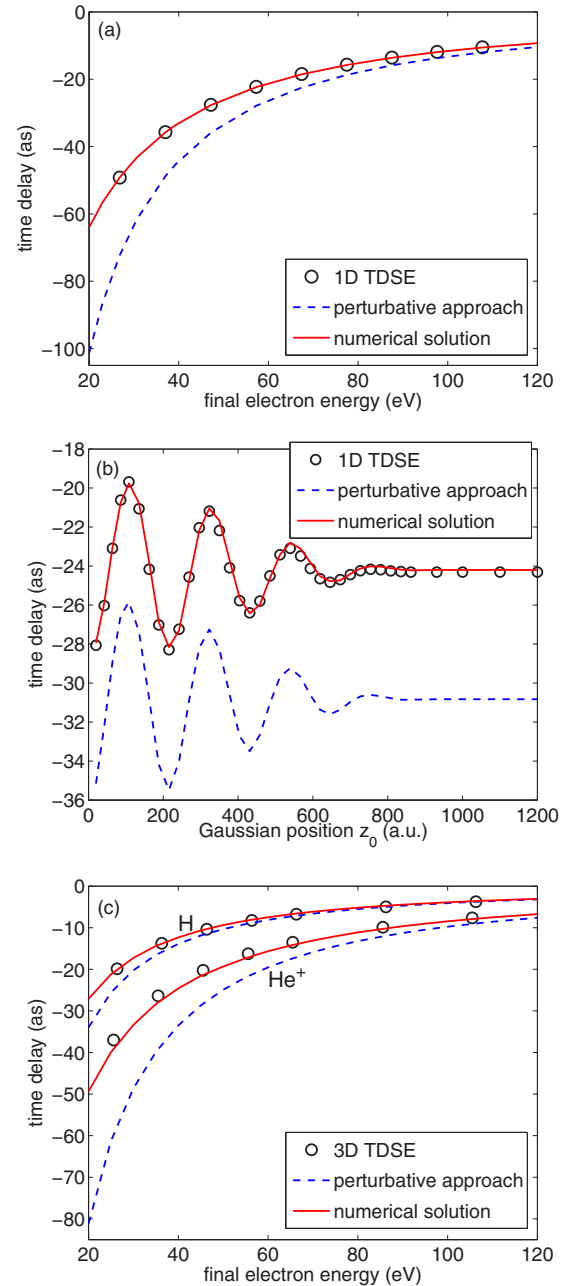


FIG. 2. (Color online) Comparison of streaking time delays from quantum streaking simulations (black circles) with classical results from the perturbative approach [dashed (blue) lines] and the full numerical solution [solid (red) lines]. In our analysis we considered three potentials: (a) the 1D Coulomb potential [$V_C(z)$], (b) the combination of 1D Coulomb and Gaussian potentials [$V_{CG}(z)$], and (c) the 3D Coulomb potential [$V(\mathbf{r})$].

each other. In the present set of calculations the difference between the quantum and the full classical results does not exceed 2 as, which shows that the numerical streaking simulations can be well analyzed and interpreted using a classical approach. Such a conclusion has also been reached based on the results of classical trajectory Monte Carlo calculations in Ref. [8]. This supports the assumptions made in the classical approach that the transition of the electron from the bound state to the

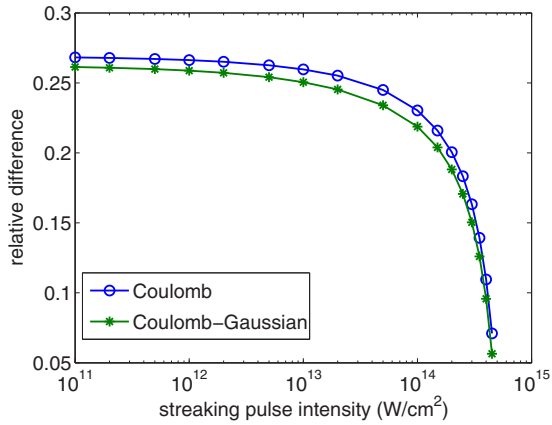


FIG. 3. (Color online) Relative difference in the momentum shift Δk calculated classically from the perturbative approach vs the full numerical solution for $V_C(z)$ [solid (blue) line with circles] and $V_{CG}(z)$ [$z_0 = 200$; solid (green) line with asterisks]. The relative difference is defined as $|(\Delta k^{(\text{pert})} - \Delta k^{(\text{numerical})})/\Delta k^{(\text{numerical})}|$. We have considered photoemission of an electron with a final asymptotic momentum of 2.0, which is streaked by a three-cycle, 800-nm laser pulse.

continuum occurs instantaneously upon application of the XUV pulse (i.e., $\tau = t_i$) and the observed temporal offset Δt_s , or time delay, arises due to the propagation of the photoelectron in the continuum.

On the other hand, the comparison further shows that the results of the perturbative classical approach [dashed (blue) lines] do not agree either with those of the quantum simulations (black circles) or with the full classical calculations [solid (red) lines]. We find discrepancies of more than 30 as compared to the quantum results and the full classical results in some of our present calculations [e.g., the low-energy part in Fig. 2(a)]. This degree of deviation between the two classical approaches persists for intensities of the streaking field up to 10^{14} W/cm². We exemplify this by showing in Fig. 3 the relative difference between the results for the momentum shift Δk , obtained from the two classical approaches for both $V_C(z)$ [solid (blue) line with circles] and $V_{CG}(z)$ [solid (green) line with asterisks]. We note that, in general, results of the perturbative approach and the full numerical solution tend to agree only for high streaking-field intensities, which would induce ionization from the target by the streaking field itself.

We can therefore further conclude that the discrepancy in the results of the perturbative classical approach versus the quantum streaking simulations does arise from the first-order approximation of the Coulomb potential, and not from the use of classical theory itself. It appears that the transition of the electron from the bound state into the continuum in photoionization occurs at distances at which the perturbation condition $|E_s| \gg |dV/dz|$ is not fulfilled for moderate streaking-field strengths. This conclusion is further supported by the results for the combination of the Coulomb and Gaussian potentials [$V_{CG}(z)$]. In this case the final time delay has two contributions, one resulting from the Coulomb potential and the other from the rather weak Gaussian potential. In test calculations we studied both contributions independently and

found that in the present results the deviation between the two classical results arises from the Coulomb potential alone. This can also be seen in the results in Fig. 2(b), as the difference between the two classical results is independent of the position of the Gaussian potential.

Before proceeding, we briefly discuss the option to extend the perturbative classical result for the analysis of streaking calculations. The deviations found for the first-order approximation can be significant. It remains to be studied if higher order corrections can improve the results sufficiently or a nonperturbative treatment becomes necessary. Alternatively, it might be more interesting to partition the space into an inner region close to the nucleus and an outer region, with $|E_s| \gg |dV/dz|$ fulfilled for the outer one. Then an application of the perturbative result for the time delay related to the outer region appears to be satisfied. We may point out that the (perturbative) eikonal approximation was indeed initially introduced in the context of strong-field ionization [25]. For strong fields, in contrast to weak-field photoionization, the perturbative condition is usually well satisfied for distances beyond the tunnel exit, at which the electron enters the continuum. Results of previous theoretical calculations [12] indicate that it might then be useful to approximate the time delay in the inner region by the WS time delay for the short-range part of the potential. Of course, the quality of such an approximation should depend on the potential of interest, the streaking-field strength, and other parameters, which would determine the partition between the inner and the outer regions and the range of the short- vs long-range parts of the potential. We did not further investigate this option, since the full classical solutions are in excellent agreement with the present quantum streaking results and therefore provide a good starting point for our further analysis.

III. FINITE-RANGE PROPERTY OF STREAKING TIME DELAYS

As discussed in the previous section, the agreement between the quantum streaking results and the full classical results obtained using Eq. (15) implies that the temporal offset in the streaking calculation arises due to the propagation of the electron in the continuum after the transition from the bound state upon an instantaneous response to the XUV ionizing pulse. Furthermore, Eq. (15) shows that the time delay depends on the finite time between the transition into the continuum and the end of the streaking pulse, which has been previously confirmed by quantum streaking simulations [21]. In this context it is also interesting to recall that within the classical analysis the time delay can be also approximated as [21]

$$\Delta t_s \simeq \sum_{j=1}^N \frac{E_s(t_j)}{E_s(t_i)} \Delta t_{\text{field-free}}^{(j)}, \quad (18)$$

where $\Delta t_{\text{field-free}}^{(j)}$ is the streaking-field-free time delay that the electron accumulates during its propagation in the time interval $[t_j, t_j + \delta t]$ and over the related finite region $[z_j, z_j + \delta z]$ of the potential compared to the propagation of a free particle over the same distance in space. This approximation shows that the piecewise field-free time delays are weighted by the instantaneous streaking-field strengths $E_s(t_j)$ relative to the

field strength at the instant of transition into the continuum, $E_s(t_i)$. We note that the oscillations of the time delays in Fig. 2(b) can be readily explained by Eq. (18); this has been observed and explained in our earlier publication [21]. In this section we analyze and discuss a few consequences of this finite-range property of the temporal offsets.

A. Variation of the time delay over different cycles of a streaking pulse

According to our analysis the time delay Δt_s depends on the time interval between transition of the electron into the continuum, t_i , and the end of the streaking pulse, T_s . We therefore expect that in a long streaking pulse the time delay, extracted from different cycles of the streaking pulse, varies, since, for emission of the electron by the XUV pulse in the rising part of the streaking pulse, it will propagate over a larger distance until the streaking pulse ceases compared to the case where the electron is released in the trailing part of the streaking pulse.

To test our expectations we have performed quantum streaking simulations for the 1D Coulomb potential $V_C(z)$, Eq. (3), and the combination of the 1D Coulomb and Gaussian potentials $V_{CG}(z)$, Eq. (16), using an eight-cycle streaking pulse. We then extracted the time delay Δt_s by fitting the streaked momentum over different intervals of the streaking pulse using Eq. (6). The results are listed in Table I, where negative times in the interval $[t_1, t_2)$ correspond to the rising part of the pulse, while positive times correspond to the trailing part of the pulse.

As expected, the extracted time delays depend on the interval used for the fitting procedure. In the case of the 1D Coulomb potential the variation of the time delays over the streaking pulse are rather small. This indicates that the major part of the time delay is accumulated shortly after the transition of the electron into the continuum near the nucleus, where the potential is strongest. On the other hand, for the combined Coulomb-Gaussian potential we see a strong change in the time delay for application of the XUV pulse at the beginning of the streaking pulse compared to the other fitting intervals. This can be understood within our interpretation of the time delay. If the electron is ionized early, it reaches the Gaussian potential during its propagation at high streaking-field strengths. According to Eq. (18), this part of the potential therefore contributes significantly to the accumulated time delay. On the other hand, if the electron is ionized later, it reaches the Gaussian potential either when the streaking pulse is weak or after the end of the streaking pulse

TABLE I. Streaking time delays for different time intervals $[t_1, t_2)$ of the streaking trace. An eight-cycle streaking pulse and two 1D potentials [$V_C(z)$ and $V_{CG}(z)$ ($z_0 = 650$)] have been used for the simulation. All values are given in atomic units.

$[t_1, t_2)$	Coulomb	Coulomb-Gaussian
$[-400, -200)$	-0.9867	-1.3855
$[-200, 0)$	-0.9985	-1.0765
$[0, 200)$	-1.0085	-1.0130
$[200, 400]$	-1.0250	-1.0250

(i.e., for the interval $[200, 400]$). In these cases the effect of the Gaussian potential on Δt_s is small or absent, in agreement with Eq. (18). The results therefore confirm the finite-range property of the observed time delays. Furthermore, they actually open the possibility of using the streaking technique to image the presence and even the position of an additional potential (here, the Gaussian potential) within a long streaking pulse.

B. Role of the polarization direction

Previously, we have considered 1D examples which have already revealed important aspects of the physics behind the streaking measurement technique. We now investigate the role of the polarization direction in view of the finite-range property of the time delay and the detection of a static potential at a distance from the location of the photoemission. To this end we consider the 2D potentials

$$V_1(x, y) = \begin{cases} -\frac{Z}{\sqrt{r^2+a}} - V_{0,1}e^{-\frac{(r-r_0)^2}{\sigma^2}} & \text{for } |x| \leq 100, \\ -\frac{Z}{\sqrt{r^2+a}} & \text{for } |x| > 100, \end{cases} \quad (19)$$

$$V_2(x, y) = -\frac{Z}{\sqrt{r^2+a}} - V_{0,2}e^{-\frac{(r-r_0)^2}{\sigma^2}} \frac{y^2}{r^2}, \quad (20)$$

where $r = \sqrt{x^2 + y^2}$. Both potentials are shown in Fig. 4 for $Z = 2.0$, $a = 0.164$, $V_{0,1} = 0.5$, $V_{0,2} = 0.25$, $r_0 = 140$, and $\sigma = 5.0$. In our calculations the electron was initially bounded in the ground state of the Coulomb potential with an eigenenergy of -2.0 . We then used an XUV pulse with $I_{XUV} = 1 \times 10^{14}$ W/cm², $\omega_{XUV} = 68$ eV, $N_{XUV} = 10$, and $\phi_{XUV} = -\pi/2$ and a three-cycle, 400-nm streaking pulse with $I_s = 1 \times 10^{12}$ W/cm² and $\phi_s = -\pi/2$ to streak the momentum of the photoelectron. The TDSE was solved using a space-time grid with $\Delta x = \Delta y = 0.3$, $N_x = N_y = 5000$, and $\Delta t = 0.05$ in 2D Cartesian coordinates. The polarization directions of ionizing and streaking pulses were kept parallel, but the polarization direction with respect to the orientation of the potentials was varied.

To obtain the streaking trace as a single curve as in Fig. 1(a), we first performed a 2D Fourier transform of the ionized part of the wave function at the end of each simulation for a given time delay between the XUV and the streaking pulses. This 2D momentum distribution was then integrated over a small opening angle ($\pm 5^\circ$) with respect to the polarization direction of the coaligned ionizing and streaking pulses, since the streaking effect is expected to be strongest along the polarization direction of the streaking pulse. Next, we obtained the expectation value of the resulting momentum distribution for a given time delay τ . Finally, by repeating the calculations for application of the XUV ionizing pulse over the central cycle of the streaking pulse we obtained the desired streaking trace as a function of the time delay between the two pulses and determined the temporal offsets by comparison with the vector potential as before in the 1D cases. We have propagated all wave packets for different XUV-streaking delays to the same distance in space, therefore the conclusions based on the qualitative behavior of the results presented below do not

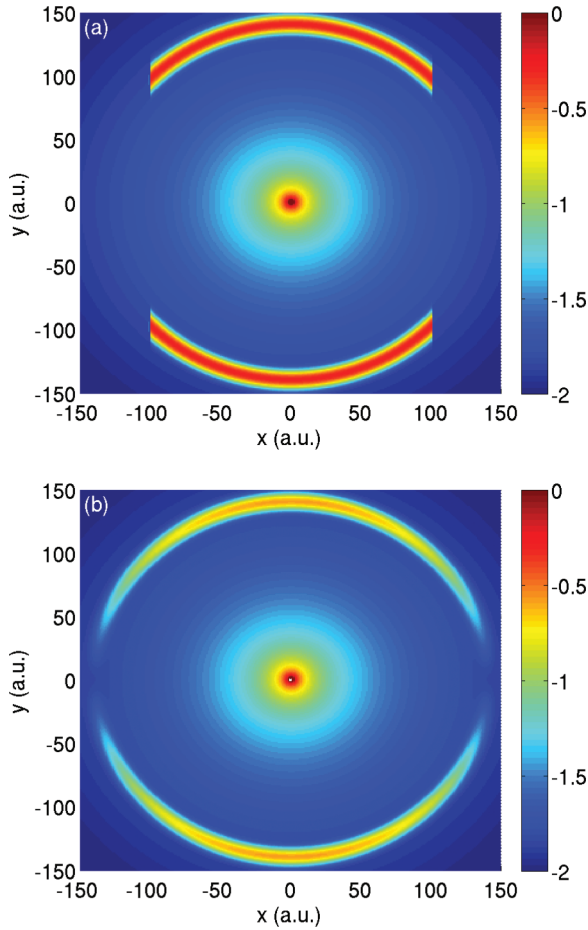


FIG. 4. (Color online) Two-dimensional model potentials, as defined (a) in Eq. (19) and (b) in Eq. (20), plotted on a logarithmic scale as $\log[-V(x,y)]$.

depend on the particular choice of wave function used for calculating the momentum distributions.

In Fig. 5(a) we present the streaking time delays as a function of the number of cycles in the streaking pulse for the 2D potential defined in Eq. (19). We compare the results obtained for the full potential in which the pulses are polarized in either the x [(green) line with asterisks] or the y direction [(red) line with squares] with those in which we neglected the additional Gaussian potential at a distance from the Coulomb potential [(blue) line with circles]. Due to the spherical symmetry of the pure 2D Coulomb potential, in the latter case the results are independent of the choice of the polarization direction and we therefore show the results obtained for polarization along the x direction only. In contrast, with the additional Gaussian potential the results strongly depend on the polarization direction. While the streaking time delays with and without additional potential agree with each other for polarization of the streaking field along the x direction, they deviate from $N = 6$ on for polarization in the y direction. The latter behavior is similar to the 1D example studied before [21]. The difference in the results is due to the fact that the time delay is determined by the photoelectron dynamics in the coupled field of the atomic potential and the streaking field along the polarization direction. For short

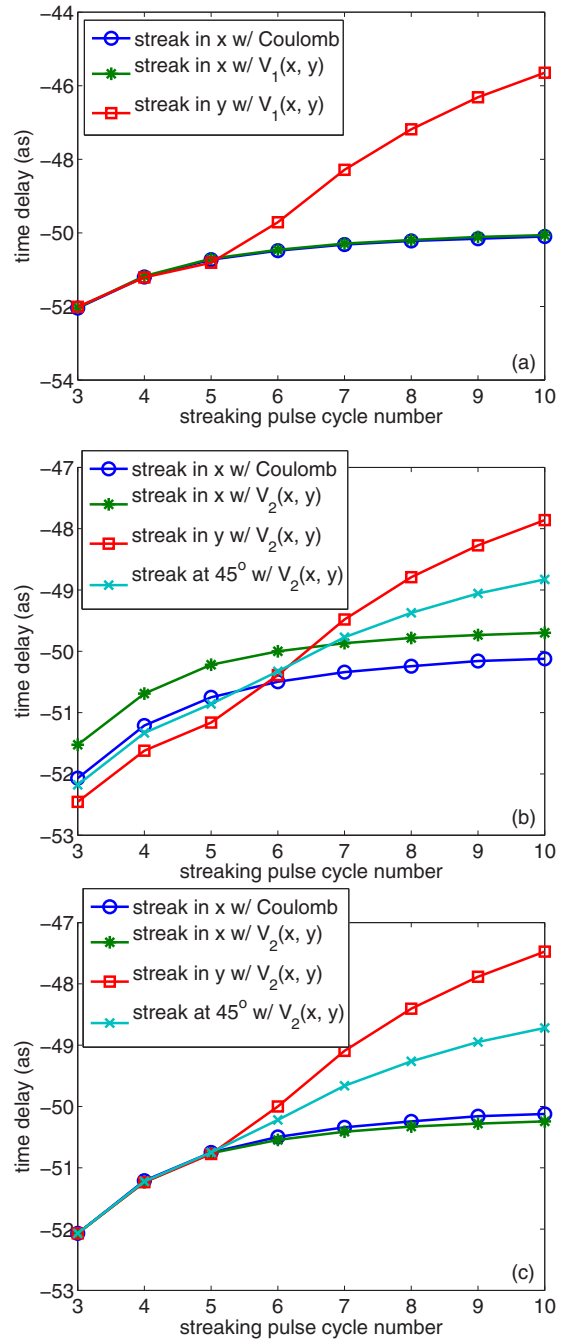


FIG. 5. (Color online) Time delay as a function of streaking-pulse cycle number for the 2D potentials defined (a) in Eq. (19) and (b, c) in Eq. (20) and polarizations of the streaking (and coaligned XUV ionizing) field in the x direction [(green) line with asterisks], at 45° [(cyan) line with crosses], and in the y direction [(red) line with squares]. The results are compared with those for the pure 2D Coulomb potential without the additional potential [(blue) line with circles] and a streaking field polarized in the x direction. In (c), the original streaking time delays for the 2D potential, Eq. (20) as shown in (b), have been shifted to match the result for the shortest streaking pulse for the pure 2D Coulomb potential.

streaking pulses the photoelectron does not reach the location of the additional Gaussian potential and the effect of the latter is therefore negligible, while for longer pulses the coupling effect between the streaking field and the additional Gaussian

potential becomes present. The additional model potential is present along the y polarization but not in the x direction, in agreement with our observations for the different polarization directions of the field.

Next, in Fig. 5(b) we show the results obtained for the second 2D potential, Eq. (20). Time delays for the full potential and different polarizations of the coaligned ionizing and streaking pulses [polarization in the x direction, (green) line with asterisks; at 45° , (cyan) line with crosses; and in the y direction, (red) line with squares] are compared with those obtained without an additional potential [(blue) line with circles]. We note that in this case the time delays do not coincide with each other, even for short streaking pulses, for which the photoelectron wave packet does not reach the additional potential when the streaking pulse ceases. Further analysis revealed that this discrepancy can be explained as being due to the scattering of the photoelectron at the additional potential, which leads to different final momentum distributions compared to that of

the pure 2D Coulomb-potential case. In order to remove this scattering effect, we shifted all time delay curves such that the results match for the shortest streaking pulse. The resulting modified time delays, shown in Fig. 5(c), then again reveal the finite-range property since the curves deviate for $N > 5$. We, furthermore, observe that the degree of deviation increases as the additional potential along the polarization direction gets stronger.

C. Shape of the streaking pulse

So far, we have considered streaking pulses with a \sin^2 envelope. According to the classical analysis, Eq. (18), however, the time delay depends on the instantaneous field strength during the propagation of the electron in the continuum. It is therefore interesting to study whether and how the shape of the streaking field envelope influences the observed time delays. In order to study this aspect we have used the following pulse envelope:

$$E_{\text{env}}(\beta_p, T_p) = \begin{cases} E_0 \sin^2(\pi t / T_s) & \text{for } 0 \leq t \leq T_s/2, \\ (1 - \beta_p) E_0 \sin^2(\pi t / T_s) + \beta_p E_0 \cos^2[\pi(t - T_s/2)/(T_s + 2T_p)] & \text{for } T_s/2 \leq t \leq T_s, \\ \beta_p E_0 \cos^2[\pi(t - T_s/2)/(T_s + 2T_p)] & \text{for } T_s \leq t \leq T_s + T_p, \\ 0 & \text{otherwise.} \end{cases} \quad (21)$$

As shown in Fig. 6 the corresponding field has a pedestal in the trailing part of the pulse, which depends on the parameters β_p and T_p . For $\beta_p \rightarrow 0$ and/or $T_p \rightarrow 0$, E_{env} equals the previously considered \sin^2 form of the envelope with duration T_s .

We performed quantum streaking simulations for different values of the parameters β_p and T_p for the 1D Coulomb potential $V_C(z)$ with effective charges $Z = 1.0$ and $Z = 3.0$, respectively, and a streaking pulse with $T_s = 331$ at a wavelength of 800 nm and a peak intensity of $I_s = 1 \times 10^{12}$ W/cm². To ionize the electron from the ground state of each potential, we have used an XUV pulse with $I_{\text{XUV}} = 1 \times 10^{15}$ W/cm², $\omega_{\text{XUV}} = 60$ eV ($Z = 1.0$) or 100 eV ($Z = 3.0$), $N_{\text{XUV}} = 10$

($Z = 1.0$) or 15 ($Z = 3.0$), and $\phi_{\text{XUV}} = -\pi/2$. In each of these simulations we extracted the time delay by applying the XUV over the interval $[0, T_s]$ of the corresponding pulse. The results are shown in Fig. 7 [solid (blue) line with circles in (a) and (c) and solid (blue) line with squares in (b) and (d)].

We observe that the time delays obtained for the pedestals deviate from those for the \sin^2 pulse shape ($T_p = 0$ or $\beta_p = 0$) for both potentials. This is in agreement with our interpretation of a finite-range time delay and the dependence on the

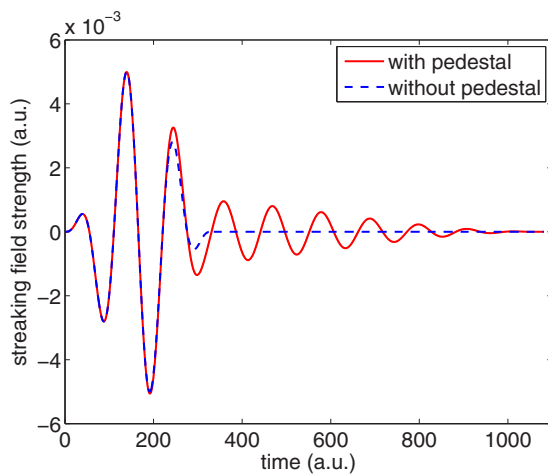


FIG. 6. (Color online) Streaking field with a pedestal [solid (red) line]: $E_0 = 5.34 \times 10^{-3}$ (i.e., $I_s = 1 \times 10^{12}$ W/cm²), $T_s = 331$, $\beta_p = 0.2$, and $T_p = 750$. For comparison, a basic three-cycle, 800-nm streaking pulse [dashed (blue) line] is also shown.

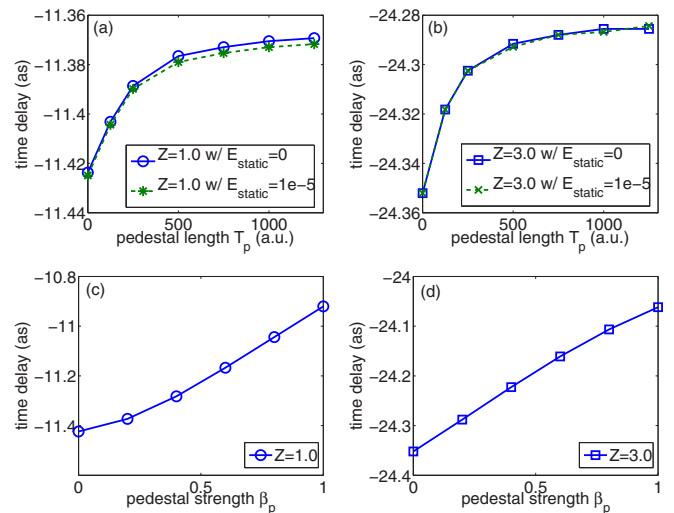


FIG. 7. (Color online) Streaking time delay as a function of (a, b) the pedestal length T_p ($\beta_p = 0.2$) and (c, d) the pedestal strength β_p ($T_p = 750$). (a, c) Results for $Z = 1.0$; (b, d) results for $Z = 3.0$. The influence of an additional static field on the streaking time delay is also present [dashed (green) lines with asterisks and crosses] in (a) and (b).

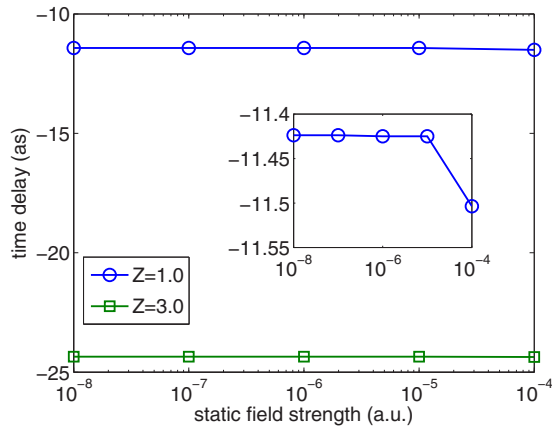


FIG. 8. (Color online) Streaking time delays as a function of the strength of the additional static field for a basic three-cycle, 800-nm streaking field for two potentials: $Z = 1.0$ [solid (blue) line with circles] and $Z = 3.0$ [solid (green) line with squares].

instantaneous streaking-field strength during the propagation of the electron [Eq. (18)], since the deviation increases as β_p or T_p increases. Quantitatively, our results, however, further show that the deviations due to the presence of the pedestal are rather small [e.g., about 1% for $Z = 3.0$ and $\beta_p = 1.0$; see Fig. 7(d)]. This is due to the fact that the effect of the pedestal comes into play when the electron is at rather large distances from the nucleus, at which the Coulomb potential is weak. Thus, we expect that for an atomic-like system pedestals and other deviations from a \sin^2 or Gaussian streaking pulse shape should not have a large effect on the observed time delays.

D. Additional static electric field

Finally, we also investigated the influence of additional static electric fields on the attosecond-streaking time delay. In an experiment the presence of such additional fields may be used in order to direct the photoelectrons towards a detector. We therefore included an additional static field term E_{static} in Eq. (1) and performed quantum streaking simulations for streaking pulses with and without pedestal. As before, we considered two 1D Coulomb potentials $V_C(z)$ with effective charges of $Z = 1.0$ and $Z = 3.0$, respectively. From the results presented in Fig. 8 we conclude that the presence of additional static electric fields up to field strengths of $E_{\text{static}} = 10^{-5}$ do not have a significant effect on the extracted time delays. The same conclusion can also be drawn for streaking pulses with a pedestal, which can be seen by comparing the dashed (green)

lines (for $E_{\text{static}} = 10^{-5}$, asterisks for $Z = 1.0$ and crosses for $Z = 3.0$) with the solid (blue) lines (for $E_{\text{static}} = 0$, circles for $Z = 1.0$ and squares for $Z = 3.0$) in Figs. 7(a) and 7(b).

IV. SUMMARY

In summary, we have theoretically analyzed the attosecond-streaking technique. To this end, we have compared the results for the time delay from quantum streaking simulations with those from two classical approximations for the dynamics of the photoelectron in the continuum, namely, a perturbative approach and the full numerical solution of the corresponding Newton's equation. We have found that the quantum and full classical results are in good agreement with each other, which shows that the time delay can be understood as being due to the dynamics of the photoelectron in the combined potential of the streaking field and the parent ion. On the other hand, the results from the perturbative classical approach deviate from both the quantum and the full classical results. Based on the interpretation that the time delay arises from the propagation of the electron in the continuum over a finite range in time until the streaking pulse ceases, we have further analyzed the role of the duration, polarization, and shape of the streaking pulse. Our results have shown that over a long streaking pulse the observed time delay can vary and that in an anisotropic potential the time delay strongly depends on the direction of the polarization and photoelectron emission. Finally, we have found that—in the case of an atomic-like potential—the shape of the streaking pulse, e.g., pedestals in the trailing part of the pulse as well as additional static electric fields, has only a small influence on the observed time delays.

ACKNOWLEDGMENTS

J.S. and A.B. acknowledge support by a grant from the U.S. Department of Energy, Division of Chemical Sciences, Atomic, Molecular and Optical Sciences Program. H.N. was supported via a grant from the U.S. National Science Foundation (Award No. PHY-0854918). A.J.-B. was supported by grants from the U.S. National Science Foundation (Awards No. PHY-1125844 and No. PHY-1068706). This work utilized the Janus supercomputer, which is supported by the National Science Foundation (Award No. CNS-0821794) and the University of Colorado Boulder. The Janus supercomputer is a joint effort of the University of Colorado Boulder, the University of Colorado Denver, and the National Center for Atmospheric Research. Janus is operated by the University of Colorado Boulder.

[1] F. Krausz and M. Ivanov, *Rev. Mod. Phys.* **81**, 163 (2009).
 [2] J. Itatani, F. Quéré, G. L. Yudin, M. Y. Ivanov, F. Krausz, and P. B. Corkum, *Phys. Rev. Lett.* **88**, 173903 (2002).
 [3] M. Schultze, M. Fieß, N. Karpowicz, J. Gagnon, M. Korbman, M. Hofstetter, S. Neppl, A. L. Cavalieri, Y. Komninos, T. Mercouris, C. A. Nicolaides, R. Pazourek, S. Nagele, J. Feist, J. Burgdörfer, A. M. Azzeer, R. Ernstorfer, R. Kienberger, U. Kleineberg, E. Goulielmakis, F. Krausz, and V. S. Yakovlev, *Science* **328**, 1658 (2010).

[4] A. S. Kheifets and I. A. Ivanov, *Phys. Rev. Lett.* **105**, 233002 (2010).
 [5] I. A. Ivanov, *Phys. Rev. A* **83**, 023421 (2011).
 [6] I. A. Ivanov, *Phys. Rev. A* **86**, 023419 (2012).
 [7] C.-H. Zhang and U. Thumm, *Phys. Rev. A* **84**, 033401 (2011).
 [8] S. Nagele, R. Pazourek, J. Feist, K. Doblhoff-Dier, C. Lemell, K. Tökési, and J. Burgdörfer, *J. Phys. B* **44**, 081001 (2011).
 [9] J. Su, H. Ni, A. Becker, and A. Jaroń-Becker, *Phys. Rev. A* **87**, 033420 (2013).

- [10] J. Su, H. Ni, A. Becker, and A. Jaroń-Becker, *J. Mod. Opt.* **60**, 1484 (2013).
- [11] M. Ivanov and O. Smirnova, *Phys. Rev. Lett.* **107**, 213605 (2011).
- [12] J. M. Dahlström, A. L'Huillier, and A. Maquet, *J. Phys. B* **45**, 183001 (2012).
- [13] J. M. Dahlström, D. Guénot, K. Klünder, M. Gisselbrecht, J. Mauritsson, A. L'Huillier, A. Maquet, and R. Taëb, *Chem. Phys.* **414**, 53 (2013).
- [14] S. Nagele, R. Pazourek, J. Feist, and J. Burgdörfer, *Phys. Rev. A* **85**, 033401 (2012).
- [15] R. Pazourek, J. Feist, S. Nagele, and J. Burgdörfer, *Phys. Rev. Lett.* **108**, 163001 (2012).
- [16] L. R. Moore, M. A. Lysaght, J. S. Parker, H. W. van der Hart, and K. T. Taylor, *Phys. Rev. A* **84**, 061404 (2011).
- [17] R. Pazourek, S. Nagele, and J. Burgdörfer, *Faraday Disc.* **163**, 353 (2013).
- [18] C.-H. Zhang and U. Thumm, *Phys. Rev. A* **82**, 043405 (2010).
- [19] J. C. Baggese and L. B. Madsen, *Phys. Rev. Lett.* **104**, 043602 (2010).
- [20] M. D. Spiewanowski and L. B. Madsen, *Phys. Rev. A* **86**, 045401 (2012).
- [21] J. Su, H. Ni, A. Becker, and A. Jaroń-Becker, *Phys. Rev. A* **88**, 023413 (2013).
- [22] E. P. Wigner, *Phys. Rev.* **98**, 145 (1955).
- [23] F. T. Smith, *Phys. Rev.* **118**, 349 (1960).
- [24] O. Smirnova, A. S. Mouritzen, S. Patchkovskii, and M. Ivanov, *J. Phys. B* **40**, F197 (2007).
- [25] O. Smirnova, M. Spanner, and M. Ivanov, *J. Phys. B* **39**, S307 (2006).